



# Catalytic properties of Au electrodes modified by an underlayer of Pd



María Fernanda Juárez<sup>a</sup>, Germán Soldano<sup>a</sup>, Hazar Guesmi<sup>b</sup>, Frederik Tielens<sup>c</sup>, Elizabeth Santos<sup>a,d,\*</sup>

<sup>a</sup> Institute of Theoretical Chemistry, Ulm University, D-89069 Ulm, Germany

<sup>b</sup> CNRS-Institut Charles Gerhardt, UMR 5253, équipe MACS, 8 rue de l'École Normale, 34296 Montpellier, France

<sup>c</sup> Sorbonne Universités, UPMC Univ Paris 06, UMR 7574, Laboratoire de Chimie de la Matière Condensée de Paris, Collège de France, 11 place Marcelin, F-75005 Paris, France

<sup>d</sup> Facultad de Matemática, Astronomía y Física, Instituto de Física Enrique Gaviola (IFEG-CONICET), Universidad Nacional de Córdoba, 5000 Córdoba, Argentina

## ARTICLE INFO

Available online 30 June 2014

### Keywords:

Gold–palladium alloys

Electrocatalysis

Density Functional Theory

Electronic structure

Hydrogen adsorption–absorption–storage

## ABSTRACT

Bimetallic catalysts have manifold technological applications; their reactivity can greatly exceed that of the original single metals. In this work, we investigate an ideal model-system consisting of a complete monolayer of Pd underneath the surface of Au(111). First, we investigate the stability of this system, and then its interaction with hydrogen. We analyze in detail the energetics and the electronic interactions for the Volmer step of the hydrogen evolution reaction (HER), and the further absorption below the surface layer of gold. We combine Density Functional Theory based on computational techniques with the theory of electrocatalysis.

© 2014 Elsevier B.V. All rights reserved.

## 1. Introduction

Bimetallic materials have attracted the attention for use in catalytic applications due to synergetic effects caused by geometric, electronic and bifunctional mechanisms [1–3]. Specially gold–palladium based alloys have been found to be good catalyst for diverse reactions such as the synthesis of vinyl acetate and acetoxylation of ethylene, which is an important chemical intermediate in the manufacture of paints [4], and the direct synthesis of hydrogen peroxide from H<sub>2</sub> and O<sub>2</sub> [5].

Palladium and gold are completely miscible as a solid solution [6]. The most common alloys are Au<sub>3</sub>Pd, AuPd and AuPd<sub>3</sub>, but they can exhibit an enormous number of possible ordered configurations with many ground states. Effectively, about 1.5 million possible structures have been investigated [7,8]. The lowest formation enthalpy is about –100 meV for the structure Au<sub>7</sub>Pd<sub>5</sub> [8]. However, the predicted ordered states of bulk Au–Pd are different from those observed in thin films. Gold shows a much lower surface energy than palladium [9]; therefore gold segregation into the surface is expected. Both experimental and theoretical results indicate segregation of gold, resulting in (nearly) pure gold in the topmost layers [10–12].

Therefore, we have to distinguish between surfaces of bulk alloys and bimetallic systems obtained by deposition of a foreign metal on a massive metallic substrate. The latter can be obtained by diverse methods, such as vacuum deposition [3], or electrodeposition under potential control in an electrochemical environment or spontaneously in a solution containing the cations of the metal [13]. Usually, a subsequent controlled annealing is performed after vacuum deposition [14] to

activate complete intermixing in the topmost layer. The resulting bimetallic surface alloys are not necessarily in thermodynamic equilibrium, but they are stable in their environment. In the case of electrochemical systems, the presence of anions can stabilize certain surface structures.

Because of its direct application in technological areas, another interesting and important field of research is the alloying phenomena in core–shell nanoparticles [15]. Moreover, the structure of nanoparticles in the nanometer size range may be controlled by several factors, which are difficult to address [16–19].

Therefore, among all the bimetallic systems, the most appropriate for basic research are *well-defined* planar single crystals with *well-defined* composition and geometrical arrangements [3,20]. They can be used as model catalysts to understand at an atomic level the diverse factors that determine reactivity [21].

The activity of nano-alloys can greatly exceed that of the original single metals. This feature indicates that the properties of the alloy surface are not a mixture of simply additional properties of both individual components, but instead genuinely bimetallic in character as pointed out by Michaelidis [22]. It is not always easy to separate all these effects. An ensemble effect is produced by a particular geometric configuration of atoms, which can favor individual steps of a reaction. Another geometric effect is the strain produced when the lattice constants of the two components are different. However, the strain can also induce electronic effects, which can hardly be distinguished from ligand or chemical effects. Both of these effects are manifested in the interatomic matrix element describing bonding interactions between an atom and its nearest-neighbors [23]. A strategy to separate the latter [24,25] is to use *artificial* lattice constants to calculate the electronic density of states and compare them with those of real systems. Therefore, electronic modifications resulting from the formation of heteronuclear metal –

\* Corresponding author at: Institut für Theoretische Chemie Universität Ulm Albert-Einstein-Allee 11 D-89081 Ulm, Germany.

metal bonds, involving either charge transfer between the metals or orbital rehybridizations, can be discriminated from electronic changes produced by expansion or contraction of the intermetallic bonds.

For a long time, the simple but elegant *rigid-band* model [26] has been applied to account for the electronic properties of alloys, although already in the sixties its limits have been recognized [27,28]. It establishes that, if its valence is greater than that of the *solvent* metal, then the only effect of the addition of a foreign metal (*solute*) is swelling the Fermi surface and filling of the density of states. Usually, many scientists have the tendency to carry simple models over *without change till one runs into difficulty, and then to stop and scratch one's head*, as nicely formulated by Stern [27]. These models involving in many cases *descriptors*-parameters are very useful to find general tendencies and therefore to give advice to experimentalists. However, in order to understand the fundamental aspects of real systems, more rigorous treatments are necessary. In the case of alloys, experimental evidence [29–32] has demonstrated that the electronic redistribution that takes place by alloying is a complicated interplay between electronic states of both components, including intra-/extra-atomic charge transfer, orbital rehybridizations and band splitting.

The intensive research of bimetallic systems involved both theory and experiments, mainly oriented to the investigation of the reactivity of nanoalloys and surface alloys [additionally to the previously mentioned works, other examples of the literature on this topic are: 33–58].

Hydrogen–metal interaction plays an important role in heterogeneous catalysis as well as in electro-catalysis. Adsorbed hydrogen is an intermediate in several processes of practical interest: it is oxidized in Fuel Cells, it is the splitting product of water electrolysis and it forms metal hydride, which can be used for storage applications.

Moreover, bimetallic systems have been widely investigated in the scope of hydrogen electrocatalysis by various groups including ourselves [3,25,33–41,44,47,52,54–59].

However, most of the bimetallic catalyst investigated for hydrogen oxidation/evolution has been overlayers of a foreign metal on a substrate.

In this work, we study the interaction of hydrogen with a bimetallic system consisting of a complete monolayer of Pd underneath the top layer of Au(111). This is an ideal model-system, which can be used as a starting point to understand the mechanisms of catalysis in bimetallic systems. Further, more complicated bimetallic arrangements shall be addressed in future works.

First, we investigate the stability of such system, and then the interaction with hydrogen when it approaches the surface and penetrates up to the second layer of the foreign atom. We analyze in details the energetics and the electronic interactions for the Volmer step of hydrogen evolution reaction (HER) and the further absorption below the surface layer of gold. We combine DFT-based computational techniques with the theory of electrocatalysis developed in one of our groups [60,61].

## 2. Computational details

The geometry optimization, the calculation of the total energy and density of states were performed using the plane-wave periodic DFT codes: Dacapo [62] and VASP [63,64]. The Kohn–Sham equations were solved within the PBE exchange–correlation functional [65,66], already used in former studies [67–69].

In the VASP calculations, the electron–ion interactions were described by the Projector Augmented-Wave (PAW) method [70,71]. The electron wave functions were expanded in a plane-wave basis set up to a kinetic energy cutoff of 400 eV. Brillouin zone integration was performed using a  $(9 \times 9 \times 1)$  Monkhorst–Pack mesh. In the calculations performed using Dacapo, an energy cutoff of 450 eV and a Monkhorst–Pack grid of  $(8 \times 8 \times 1)$  were used [72–74]. The systems are not magnetic, though when the hydrogen atom is farther than 2.2 Å from the surface, it becomes spin polarized. Therefore, spin was only considered for the latter case.

The plane wave energy cutoff and the k-point mesh were chosen by optimizing the properties of the bulk system. The lattice constants calculated from the equilibrium geometry of a periodic fcc bulk structure were 3.99 Å for Pd, and 4.18 Å for Au, which are in agreement with the experimental values (3.88 and 4.07 Å [66], respectively).

The surface was modeled according to the following procedure. Four layers of gold with a (111) surface geometry were used as a substrate. Over these layers, a layer of Pd and another of Au were added, reproducing the geometry of a (111) surface. In the resulting slab, the bottom two layers of Au were constrained at the bulk geometry. A vacuum corresponding to five layers (or 18 Å) was used in all systems.

For the study of the hydrogen adsorption and absorption, two different coverages were used: 1.0, and 0.25 monolayers (ML). The unit cells used to reproduce these coverages were  $(1 \times 1)$  and  $(2 \times 2)$  with one hydrogen atom, respectively. Once again, the geometry optimization was performed keeping fixed the bottom two layers of gold.

The studied systems were relaxed until the convergence criterion was achieved, i.e. when the total forces were less than 0.01 eV/Å

## 3. Results and discussion

### 3.1. Structural, electronic and energetics changes induced by Pd underneath the surface of Au(111)

Fig. 1 shows the structure of the bimetallic system investigated in this work (called **Au/Pd/Au(111)**) and different additional related systems used for the calculations.

VASP and DACAPO calculations carried out for the *real* Au(111) system (called **Au/Au/Au(111)-II**) yield after relaxations the following results (values obtained by DACAPO in brackets): the first Au neighbor distance is 2.94 Å and the distance between the first and second surface layers is 2.40 Å (2.43 Å). In the Pd(111) system (not shown in Fig. 1), the first Pd neighbor distance is 2.80 Å and the distance between the first and second surface layers is 2.28 Å (2.30 Å).

The substitution of the gold second layer of Au(111) by a monolayer of Pd induces strong contractions in the slab, mainly in the z-direction perpendicular to the surface. The Pd layer is at 2.29 Å (2.30 Å) from the top most surface Au layer and at 2.27 Å (2.29 Å) from the underlayer of Au, which approaches the distances in Pd(111). However, the pseudomorphic Pd layer is expanded in the xy-plane in comparison with the one-component system Pd(111). Effectively, Pd atoms have three gold first neighbors at 2.85 Å (2.86 Å) and three gold second neighbors at 2.86 Å (2.87 Å), but six palladium third neighbors at 2.96 Å (2.96 Å), similarly to the one-component system Au(111).

The formation energy  $\Delta E_f$  of the bimetallic system was calculated using the following expression:

$$\Delta E_f = E(\mathbf{Au/Pd/Au(111)}) + E(\mathbf{Au_{bulk}}) - [E(\mathbf{Au/Au/Au(111)-II}) + E(\mathbf{Pd_{bulk}})]. \quad (1)$$

The resulting sub-monolayer is stable, as indicated by the negative value obtained by VASP:  $-0.07$  eV/atom; values of the same order were obtained by DACAPO. Important to notice is that the energy needed for taking Au and Pd atoms from their bulk is compensated by the tendency of the AuPd system to maximize Au–Pd interactions. This is in line with the bulk phase diagram where a total miscibility is found for this alloy [7]. In addition, Au has a lower surface energy than Pd, and in consequence Pd underlayers are more stable than Pd overlayers. The calculated formation energy for a whole overlayer of Pd was of about  $0.2$  eV/atom. The positive formation energy of a Pd monolayer seems to suggest that under potential deposition (upd) of Pd is not possible; this is contradictory to experiments. However, it is well known that the presence of anions in the electrochemical environment can stabilize certain structures that are unfavorable in vacuum [13]. We can also notice that the segregation energy of a monolayer of Pd from the second to the first layer of the slab i.e. the energy difference between

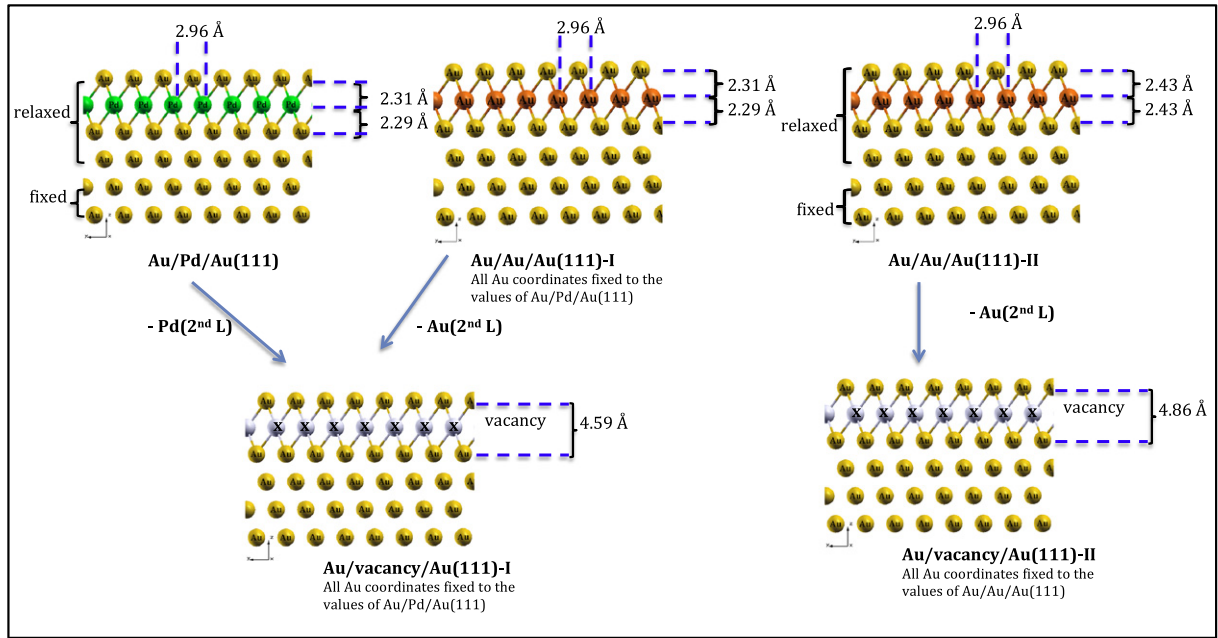


**Fig. 1. Au/Pd/Au(111):** Bimetallic system where the first layer of Au, the second layer of Pd, the third and fourth layers of Au were relaxed, while the two deeper layers of Au have been fixed to the bulk coordinates of Au(111). *Fictitious Au/Au/Au(111)-I:* Au(111) where the coordinates of all layers were fixed to those of the system Au/Pd/Au(111). *Au/Au/Au(111)-II:* real Au(111) system, where the coordinates of the fourth surface layers were relaxed and the two deeper layers were kept fixed to the bulk coordinates of Au(111). *Fictitious Au/vacancy/Au(111)-I:* system Au/Pd/Au(111)/Au/Au/Au(111)-I without the second layer of Pd/Au with all Au coordinates fixed to the values of Au/Pd/Au(111). *Fictitious Au/vacancy/Au(111)-II:* system Au/Au/Au(111)-II without the second layer of Au with all Au coordinates fixed to the original system.

the system with Pd substituted first layer and system with Pd substituted second layer, is of  $\Delta E_{\text{seg}} = 0.359$  eV/atom. This value is similar to the DFT calculated segregation energy of one Pd impurity in gold matrix [42, 43].

The binding energy between Au and Pd was calculated as following:

$$\Delta E_{\text{bind}}(\text{Au-Pd}) = E(\text{Au/Pd/Au(111)}) - E(\text{Au/vacancy/Au(111)-I}) - E(\text{Pd}(2^{\text{nd}}\text{L})) = -2.055 \text{ eV.} \quad (2)$$

The first term corresponds to the energy of the bimetallic system relaxed as indicated in Fig. 1. The second term is the energy of the bimetallic system without the second Pd layer, but with the coordinates of the Au layers fixed to the values obtained relaxing the whole bimetallic system. The third term is the energy of a single Pd layer with the coordinates fixed to those of the relaxed Pd layer in the bimetallic system (also see Fig. 1 for more details about the structures and relaxations). Similarly, we have performed the same calculation, but using one layer of Au atoms instead of Pd atoms:

$$\Delta E_{\text{bind}}(\text{Au-Au}) = E(\text{Au/Au/Au(111)-II}) - E(\text{Au/vacancy/Au(111)-II}) - E(\text{Au}(2^{\text{nd}}\text{L})) = -0.973 \text{ eV.} \quad (3)$$

Here, we have fixed all coordinates to those of the relaxed Au(111) system (see Fig. 1 for more details).

Obviously, in both cases the binding energies are negative, although that corresponding to the bimetallic Pd–Au system is almost 1 eV lower. As we have pointed out above, the surface energy of Au is lower than that of Pd. Furthermore, due to relativistic effects that we have taken into account in the pseudopotentials, Au planar structures are considerably more stable than Pd planar structures. Therefore, Au isolated monolayers are more stable than those of Pd. Then, one expects a less negative binding energy for Au than for the Pd–Au bimetallic systems. However, it does not explain the 1 eV difference. This result clearly indicates that the binding energy between Pd and Au is much stronger than that between Au and Au.

The effect on the distribution of electronic charge when the Au-atoms of the second layer of Au(111) are replaced by a monolayer of Pd-atoms can be investigated from different points of views. While in the case of density of states the redistribution in energy can be analyzed, the charge difference characterization gives a description of the redistribution in space. In latter case, an important issue is the selection of the reference systems. The changes produced in energy of the density of states allow identifying, which orbitals participate in the bonds, and which rehybridizations take place.

In Fig. 2 the redistribution charge in space can be observed, when the bimetallic system is formed. In the upper part left, the 3D-isosurfaces are shown, and in the bottom the corresponding  $xy$ -planar averaged charge density. The first has been obtained according to the following expression [75–77]:

$$\Delta\rho(x, y, z)_{\text{Au-Pd}} = \rho_{\text{Au/Pd/Au(111)}} - \rho_{\text{Au/vacancy/Au(111)-I}} - \rho_{\text{Pd}(2^{\text{nd}}\text{L})} \quad (4)$$

where  $\rho_{\text{Au/Pd/Au(111)}}$ ,  $\rho_{\text{Au/vacancy/Au(111)-I}}$  and  $\rho_{\text{Pd}(2^{\text{nd}}\text{L})}$  are the spatial electron charge density distributions of the relaxed bimetallic system, the Au(111) system without the second layer of Au with the coordinates fixed to the relaxed bimetallic system, and the isolated second layer of Pd with the coordinates of Pd in the bimetallic system (also see Fig. 1).

The averaged charges in the  $xy$ -plane parallel to the surface are obtained by integration of Eq. (4) over the unit cell [76]:

$$\Delta\rho(z)_{\text{Au-Pd}} = \int_{\text{unit cell}} \Delta\rho(x, y, z) dx dy. \quad (5)$$

A complicated oscillating pattern is observed, which reflects the complex interplay between electronic states of both metallic components of the alloy. An accumulation of electronic charge is observed directly on the metal atoms of Au and Pd. This is slightly larger on Au atoms at the surface layer (see the positive peak at  $z = 0$ ) than on the Pd atoms of the second layer and decreases for the inner layers of Au (see black arrows). This result is in line with the higher electronegativity of Au compared to Pd. Between the metallic layers, electronic depletion occurs near the metal atoms and an accumulation appears in the

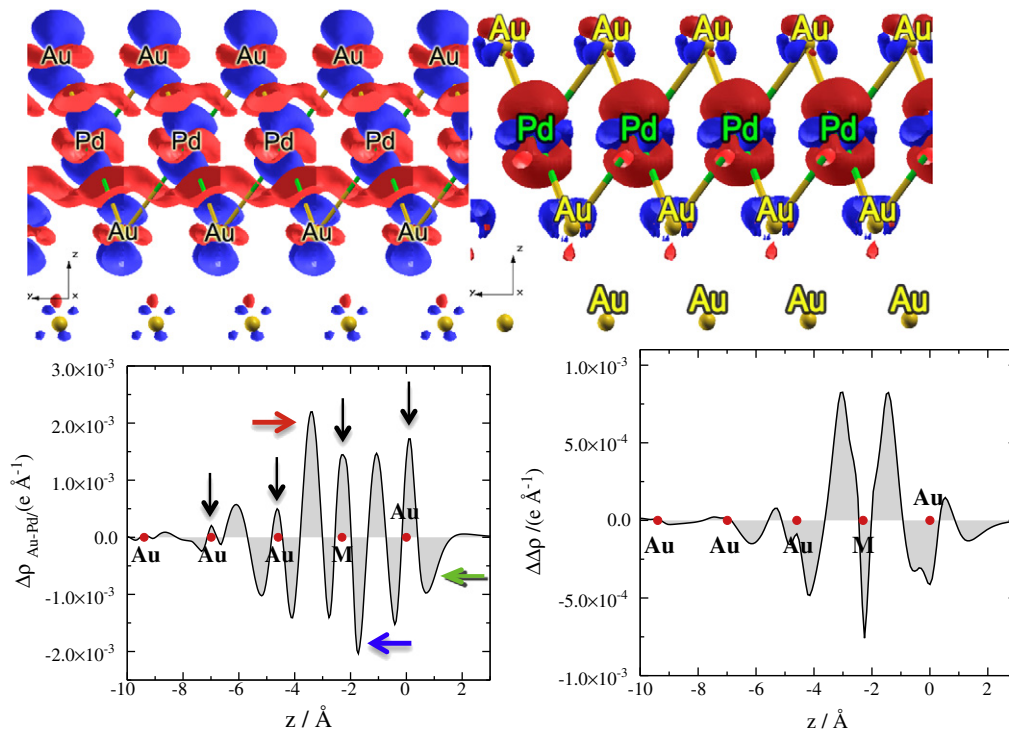


**Fig. 2.** Upper part, left: Redistribution of charge after the formation of a whole underlayer of Pd below the surface of Au(111) as obtained from Eq. (5). Isosurface  $0.002 \text{ e } \text{Å}^{-3}$ . Bottom part, left: Planar averaged charge density change as a function of the  $z$ -coordinate perpendicular to the surface obtained by integrating the electron density difference shown at the upper part over the  $xy$ -plane (Eq. (6)). Upper part, right: Difference between the redistribution of charge after the formation of a whole underlayer of Pd below the surface of Au(111) and the formation of the second layer of Au(111) with the coordinate of the bimetallic system ( $\Delta[\Delta\rho(x, y, z)_{\text{Au-Pd}} - \Delta\rho(x, y, z)_{\text{Au-Au}}]$ ). Isosurface  $0.001 \text{ e } \text{Å}^{-3}$ . Bottom part, right: Planar averaged of the difference shown in the upper part as a function of the  $z$ -coordinate perpendicular to the surface obtained by integrating the 3D plot. Red and blue colors correspond to electron accumulation and depletion, respectively. Isosurfaces have been plotted with the XCrySDen package [77].

middle. This depletion is slightly larger near the Pd atom on the right side nearer to the surface (blue arrow). On the contrary, the accumulation is slightly larger between the second layer of Pd and the third layer of Au (red arrow). The electronic charge of the deeper Au layer is more weakly perturbed and finally, the accumulation–depletion oscillations are strongly attenuated in the bulk layers. These features are evident from the 3D-isosurfaces (Fig. 2 upper-left), but they become more evident from the averaged charges plotted along the  $z$ -coordinate perpendicular to the surface (Fig. 2 bottom-left).

As a consequence of the formation of the bimetallic system, a dipole pointing from the surface is created as can be observed from Fig. 2. Therefore, a decrease on the work function occurs from 5.21 eV (value for the single metal Au(111) system) to 5.14 eV for the bimetallic Au/Pd/Au(111) system (see Table 1). Particularly the slight electronic charge depletion at distances farther out to the surface (green arrow) strongly contributes to the observed work function decrease as has been pointed out for other metallic systems [76,78]. It is sufficiently far from the surface to determine the sign of the dipole. We have to recall, that the dipole is weighted by the distance from the center of the slab.

Nevertheless, the work functions for Pd(111) and Au(111) are very similar, therefore no significant changes are expected. Furthermore, the work function of the systems presently considered is hard to

compare with experimental values because the magnitude of the variety of morphology and anisotropy. Most alloys have a measured work function different from that of the weighted average of the two component elements [79]. From experimental studies of pseudomorphic layer-by-layer Au growth on Pd(111) Fischer and Fauster [80] show a strong dependence of the work function with annealing treatment. These authors found a minimum for the work function at 800 K, which they ascribed to a surface state of Au shifting in energy and crossing the Fermi level [80]. This transition from an occupied to an unoccupied surface state obviously changes the surface dipole considerably. A decrease of the work function with the removal of electrons from this surface state induces a shift of the mean charge distribution into the front of the surface.

As we have already mentioned above, the reference systems are very important to interpret the charge difference plots. In order to appreciate the electronic charge interchange between Au and Pd, we have performed the following estimation. First, we have calculated the electronic redistribution for an *artificial* Au(111) system with the coordinates of the relaxed bimetallic system. We have used Eqs. (4) and (5) but replacing the second layer of Pd by Au. We have kept the position of the Au atoms at same relaxed coordinates obtained for the bimetallic system Au–Pd.

$$\Delta\rho(x, y, z)_{\text{Au-Au}} = \rho_{\text{Au/Au/Au(111)-I}} - \rho_{\text{Au/vacancy/Au(111)-I}} - \rho_{\text{Au(2ndL)}} \quad (6)$$

The obtained patterns are similar to those shown on the left side of Fig. 2, but with subtle variances.

Therefore, in order to understand these changes we calculate the difference between both *spatial* charge differences:  $\Delta[\Delta\rho(x, y, z)_{\text{Au-Pd}} - \Delta\rho(x, y, z)_{\text{Au-Au}}]$  and their averaged charges in the  $xy$ -plane parallel to the surface by integration. Consequently, we obtain a comparative outlook of the strength of electron drift towards the bonds Au–Au or Au–

**Table 1**  
*d*-Band-center and work function for the investigated systems.

System	$\epsilon_c^d(\text{Au})/\text{eV}$	$\epsilon_c^d(\text{Pd})/\text{eV}$
Single metals	−3.51	−2.21
Bimetallic Au–Pd	−3.29	−2.00
Artificial Pd		−1.49
$\Phi(\text{Au}) = 5.21 \text{ eV}$ ; $\Phi(\text{Pd}) = 5.31 \text{ eV}$ ; $\Phi(\text{Au-Pd}) = 5.14 \text{ eV}$		

Pd. These results are shown on the right hand side of Fig. 2. The electron density between the first and second and the second and third layers is larger for the Pd–Au bimetallic system than for the pure Au system, which is in agreement with the strength of the bond, as already determined by the energy calculations given above. Both Au and Pd contribute strongly to this interlayer electronic charge than in the case of the one component system Au(111).

The effect on the density of electronic states and their redistribution in energy of replacing the Au-atoms of the second layer of Au(111) by a monolayer of Pd-atoms can be observed in Fig. 3. Both *sp*- and *d*-bands of Au lie at lower energies than those of Pd for the one-component systems. The *sp*-band of the top layer of Au(111) starts at about  $-9$  eV below the Fermi level, while that of the second layer of Pd(111) at about 2.5 eV higher energies. In this way, between  $-9$  eV and  $-7.5$  eV below the Fermi level there is no any overlap between the *sp*-electronic states of both metals.

In the bimetallic system, the density of states corresponding to the *sp* band of the Au atoms at the surface shift to more positive energies, while those of the *sp* band of Pd atoms of the underlayer shift to negative values in comparison to the one component systems (Fig. 3). This is an effect to maximize the overlap in order to stabilize the bond between Au and Pd.

Therefore the resulting bimetallic system shows strong mixing of the *sp* bands practically forming a common band. In the case of the *d*-bands for the one-component systems, no coincidence of the position of

electronic states can be observed neither in the range between  $-7$  and  $-5$  eV below the Fermi level nor near the Fermi level ( $-1.5$  to  $0$  eV). Therefore, the *d*-bands of both Pd and Au also show a redistribution of the electronic states in order to reach a better overlap. As a consequence, the center of the *d*-bands shifts to more positive values for both metals (see dashed lines in Fig. 3 and the corresponding values in Table 1). The Pd underlayer is laterally expanded in the Au matrix because of the smaller lattice constant in comparison to Au ( $a_{\text{Pd}} = 3.89$  Å and  $a_{\text{Au}} = 4.08$  Å). Consequently, a thinner *d*-band is expected, since the electronic states become more localized.

However, the chemical interaction effects on the electronic structure are also very important. Similarly as in the case of other bimetallic systems [23–25], the electronic changes due to strain can be distinguished from those due to the proximity of the foreign atom to the substrate by detailed comparisons of *theoretically* expanded Pd(111) with the Pd/Au(111) bimetallic system. We have also implemented this strategy in a previous work [25], which has allowed us to separate these two effects. In the present work, we have calculated the density of states for the *sp*- and *d*-band of a fictitious system consisting of a slab of Pd(111) with the lattice constant of Au. Thus, only the geometrics become evident. The dashed blue line in Fig. 3 shows the result. For the artificial expanded Pd system, the shape of the bands maintains, but they both shifts upwards in energy. As expected, the *d*-band also becomes thinner.

This feature of the distribution of electronic states markedly differs of that obtained with the *real* bimetallic system (green line).

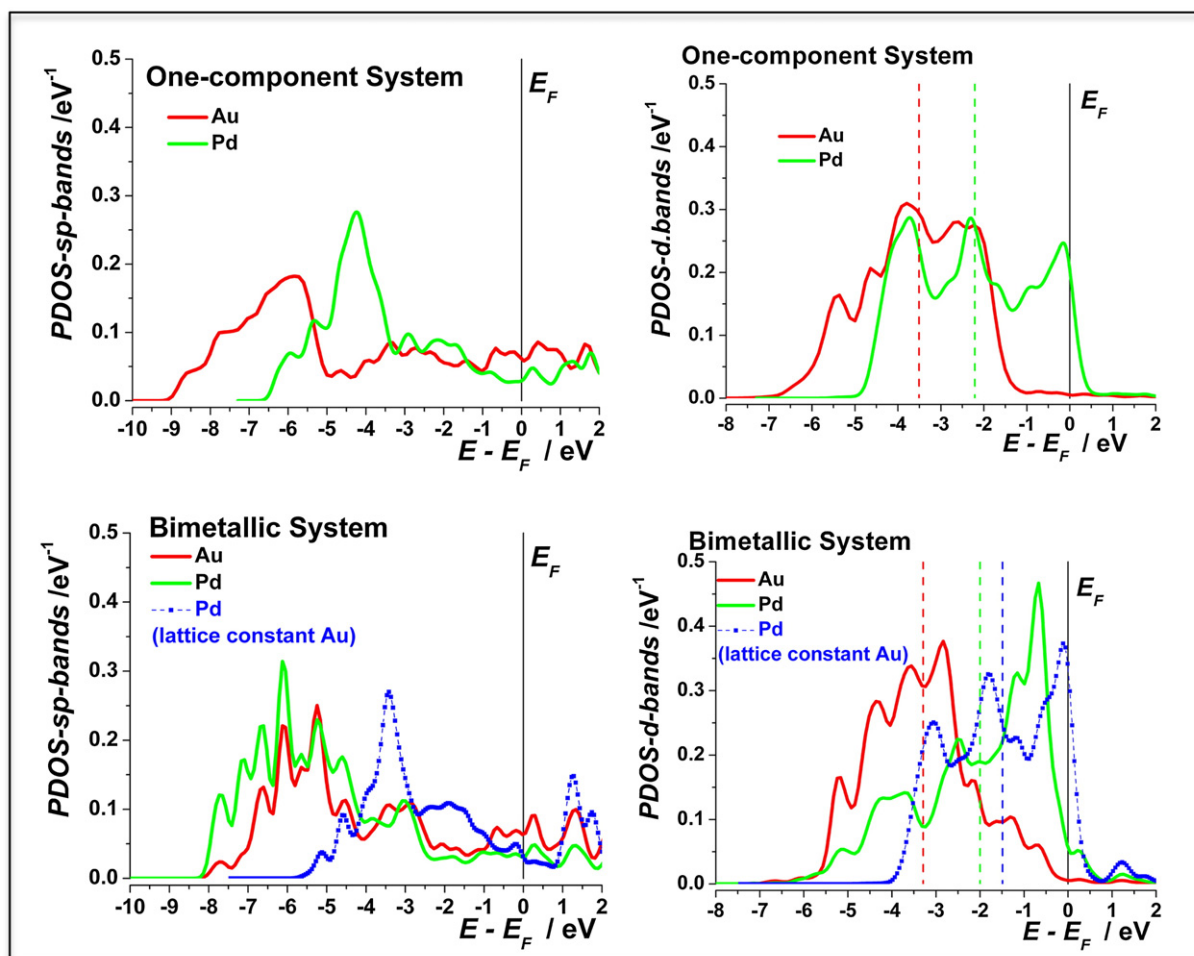


**Fig. 3.** Density of electronic states projected (PDOS) onto the *sp*-band (left) and the *d*-band (right) of the gold surface atoms (red lines) and palladium second layer atoms (green lines) for the one-component systems before the alloy formation (upper part) and for the bimetallic system after the replacement of the second Au layer by the Pd monolayer (bottom part). The blue lines with symbols correspond to the *sp*- and *d*-bands of the second layer of an artificial system of Pd(111) calculated with the lattice constant of Au. The vertical thin black lines indicate the position of the Fermi level, while the dashed red, green and blue vertical lines indicate the center of the *d*-band for Au, Pd and the artificial Pd systems respectively.

The *sp*-band of Pd displaces downwards in energy and its shape overlap very well with the *sp*-states of Au. The *d*-band of Pd shows a more complicated behavior. It is displaced upwards in energy, but less than predicted by geometric effects. Also the shape of the *d*-band is completely different, indicating that the Au–Pd chemical interactions play an important role in the changes of the electronic properties. The *d*-band of

the Au atoms at the surface also strongly changes. Now, electronic states near the Fermi level appear (see the increase between  $-1$  and  $0$  eV), which suggests that such system could be a good catalyst.

A more detailed analysis of the components of the *d*-bands of Au and Pd (see Fig. 4 and also supporting information SI-*d*-bands-components for more details) shows that the more important changes occur in the

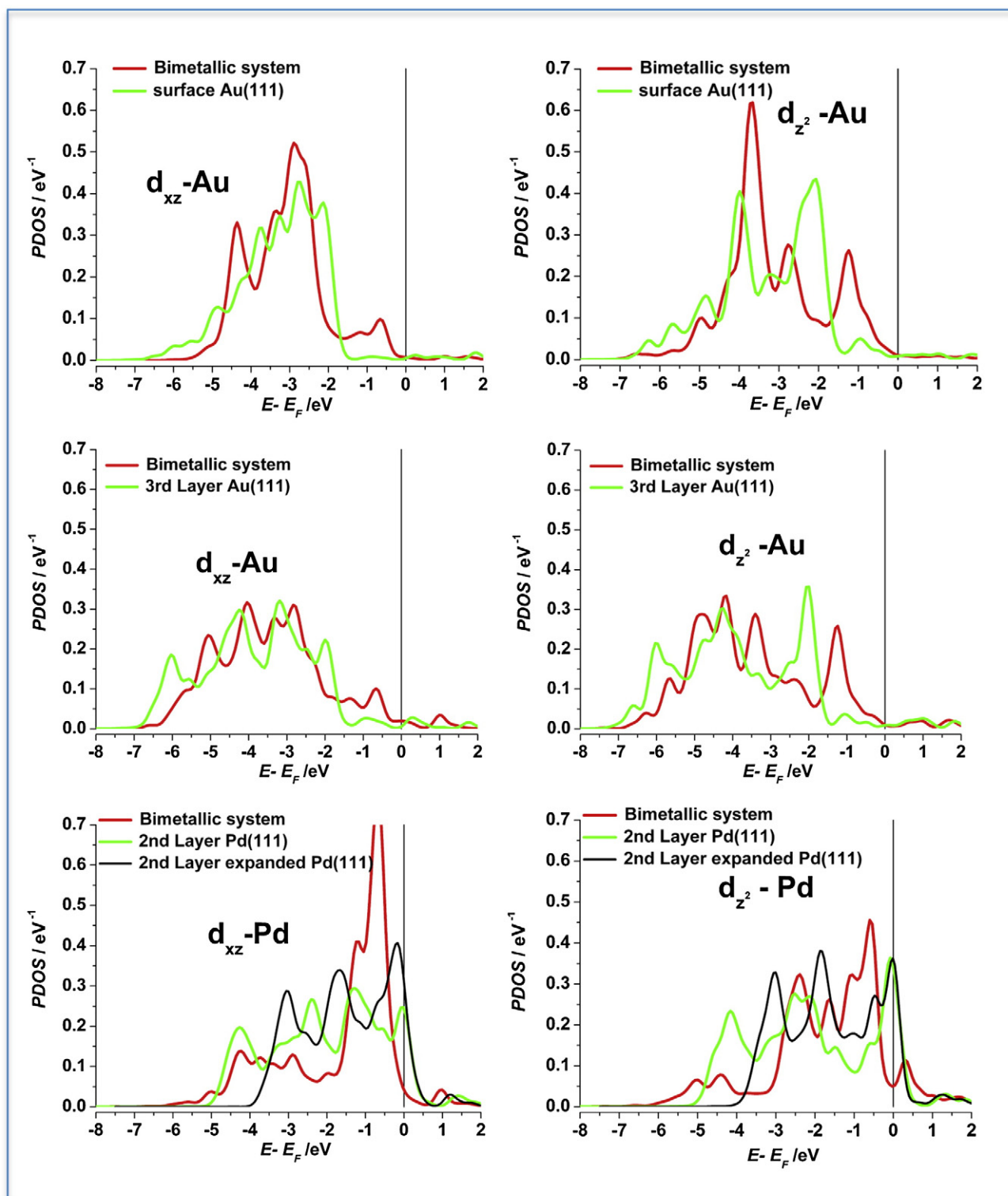


Fig. 4.  $d_{xz}$  and  $d_{z^2}$  band components projected onto Au atoms at the surface, Pd atoms of the second layer and Au atoms of the third layer (below Pd layer).

orbitals perpendicular to the surface ( $d_{z^2}$ ,  $d_{xz}$ ,  $d_{yz}$ ). The peak at about  $-1.8$  eV of the  $d_{z^2}$  of Au atoms at the surface and in the 3rd layer below the Pd layer, split into two components at lower and higher energies.

This split is less pronounced in the  $d_{xz}$ ,  $d_{yz}$  states. No considerable changes in the others orbitals are observed. In the case of the  $d_{z^2}$ ,  $d_{xz}$ ,  $d_{yz}$  electronic states of Pd, the redistribution is different and more complicated. A sharp peak appears at about  $-0.6$  eV, which overlaps very well with the new states of Au near the Fermi level. There is a slight increase in the occupation of these states (about 4%). Due to the lateral expansion, the  $d_{xy}$ ,  $d_{x^2-y^2}$  components become thinner and their shapes are similar to those of the *artificially* expanded Pd(111) system (see supporting information SI-*d*-band-components for more details).

Experimental data [29–32] obtained by X-ray absorption near-edge structure (XANES) and by core-level shifts of X-ray photoelectron spectroscopy (XPS) with Pd–Au alloys indicate a decrease in the *d* charge and a gain of *sp* charge at the Au site, while Pd gains *d* charge and loses *sp* charge. In agreement with the higher electronegativity of Au than Pd, the authors found a small net charge transfer from Pd sites to Au sites. Our calculations support these experimental results, although the changes on the occupation are not considerable. Therefore, these effects are not so strong as in the case of Pt–Sn intermetallic compounds previously investigated [38]. However, as can be inferred from Figs. 3–4, it is difficult to distinguish charge transfers because of the internal redistribution of the electronic density when the rehybridization to form the alloy takes place.

### 3.2. Energetics of hydrogen adsorption and absorption

In order to test the catalytic properties of the Au–Pd bimetallic system, the adsorption and absorption of hydrogen have been investigated. Table 2 shows the energies obtained for the adsorption and absorption on different sites, calculated by the following expression:

$$\Delta E_{\text{ads/abs}} = [E(\text{H-Au/Pd/Au(111)}) - (E(\text{Au/Pd/Au(111)}) + 1/2E(\text{H}_2))]. \quad (7)$$

Here, the first term corresponds to the energy of the relaxed system **H-Au/Pd/Au(111)** with the hydrogen at the adsorption (absorption) equilibrium position at the surface (under the first Au layer) of the **Au/Pd/Au(111)** system; the second term corresponds to the energy of the relaxed system **Au/Pd/Au(111)** without hydrogen; the third term is half the energy of a hydrogen molecule in vacuum.

In a previous work [40], we have calculated the adsorption energy for hydrogen on the more stable position fcc sites on Au(111), Pd(111) and on one monolayer of Pd on the Au(111) surface at a

coverage of  $\theta = 0.11$ ; the obtained values were 0.12 eV,  $-0.60$  eV and  $-0.66$  eV respectively.

The catalytic activity for hydrogen adsorption of the present bimetallic system (one monolayer of Pd below the first Au layer of Au(111)) seems to be only slightly lower than for the single metal systems Au(111) (Table 2).

The absorption energies obtained for the fcc and hcp sites of Pd(111) were  $-0.25$  eV and  $-0.23$  eV respectively at  $\theta = 1.0$  [82], much more favorable than the present bimetallic system. For the bimetallic system, absorption is favored over the adsorption, particularly at low hydrogen coverages (see Table 2). We shall return to this point below, where a more extensive analysis of the absorption process shall be made.

There is a large difference between hcp and fcc absorption sites. The only exothermic process is the absorption in the fcc site at low coverage. In contrast, the absorption in fcc sites is highly endothermic and therefore an unfavorable process. This difference is explained in terms of the interactions with first neighbors of hydrogen as it is illustrated in Table 2, on the right side. Hydrogen interacts more favorably with the foreign metal (Pd) than with Au. In the case of the hollow-fcc site, the next-neighbors of hydrogen are three foreign metals and one gold atom, while in the case of the hollow-hcp site, are three Au atoms and only one foreign metal next to the hydrogen.

The change in the work functions at high hydrogen coverage has been also calculated and it is shown in Table 3. As expected, the adsorption of hydrogen lowers the work function of the surface, whereas its absorption increases it. These changes are similar to those observed on Ag surfaces in a previous work [79] and are related to the electronic charge redistribution, as we shall discuss in the next section.

### 3.3. Kinetics and reaction paths for the adsorption and absorption of hydrogen

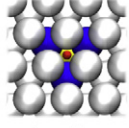
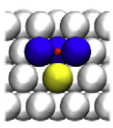
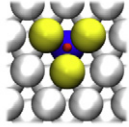
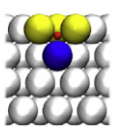
In order to investigate the kinetic processes for the adsorption and absorption of a hydrogen atom, the free energy surface as a function of the H-metal distance and the solvent coordinate representing the fluctuation on solvation configuration has been calculated. Fig. 5 shows the relative positions of the electronic states of the hydrogen atom at large distances and those of the substrate (*sp*- and *d*-bands of Au and Pd atoms at the surface and in the second layer, respectively).

In the case of the adsorption process, the Volmer step has been also considered, i.e. the electrochemical reduction of a solvated proton to produce an adsorbed hydrogen atom at the surface ( $\text{H}^+_{\text{solv}} + \text{e}^- \rightarrow \text{H}_{\text{ads}}$ ). The potential energy surface (Fig. 6) has been calculated within the framework of the electrocatalysis theory developed previously by the Ulm group's [60,61]. Distinctly from pure DFT calculation, electron transfer processes, electrochemical potential and solvent effects are explicitly considered in this theory.

Briefly, this theory combines elements of the Anderson–Newns model for the adsorption and the interactions with the electronic states of the metal [82,83], the Marcus–Hush theory for the electron transfer process in the presence of a solvent [84,85], and input parameters obtained from DFT calculations. One of these parameters is the density of states projected (PDOS) onto the 1s orbital of the hydrogen atom at the different approach distances. According to the electrocatalysis

**Table 2**

Left: Energy for hydrogen adsorption/absorption at different coverages  $\theta_{\text{H}}$  on the bimetallic system Au(111)–Pd-underlayer. Right: Illustration of the absorption sites for hydrogen in the bimetallic system. The first neighbors of H (red) are colored according to the element type, blue for Pd and yellow for Au. brg: bridge sites.

$\theta_{\text{H}}$	Site	Energy / eV	Absorption hollow-fcc	
1.00	fcc <sub>ads</sub>	0.26		
	hcp <sub>ads</sub>	0.30		
	brg <sub>ads</sub>	0.35		
	top <sub>ads</sub>	0.56		
	fcc <sub>abs</sub>	0.04		
	hcp <sub>abs</sub>	0.49		
0.25	fcc <sub>ads</sub>	0.08	Absorption hollow-hcp	
	hcp <sub>ads</sub>	0.15		
	brg <sub>ads</sub>	0.18		
	top <sub>ads</sub>	0.35		
	fcc <sub>abs</sub>	-0.20		
	hcp <sub>abs</sub>	0.33		

**Table 3**

Changes of the work function  $\Delta\Phi$  for single hydrogen ab/adsorption. The reference is the work function of the corresponding clean alloy surface.

$\theta_{\text{H}}$	Site	$\Delta\Phi/\text{eV}$
1.00	fcc <sub>ads</sub>	-0.41
	hcp <sub>ads</sub>	-0.32
	brg <sub>ads</sub>	-0.10
	top <sub>ads</sub>	-0.08
	fcc <sub>abs</sub>	0.35
	hcp <sub>abs</sub>	0.16

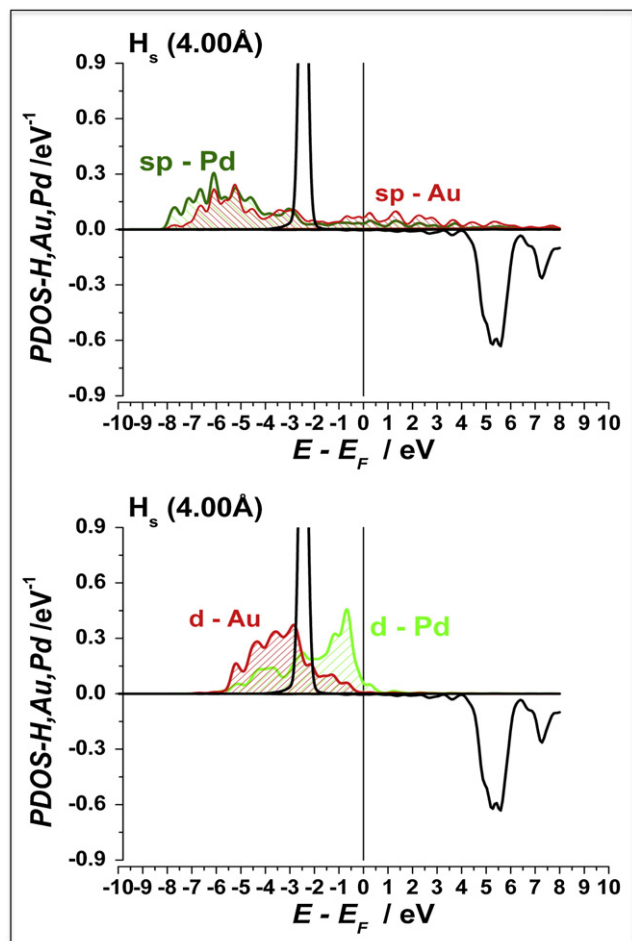


**Fig. 5.** Density of states projected onto the 1s orbital of the hydrogen atom (both spins: ↑ upper black line, ↓ lower black line), onto the *sp*- and *d*-bands of Au atoms at the surface (red lines) and Pd atoms of the second layer (green lines), when the hydrogen atoms stay at a large distance from the surface of the bimetallic system. The vertical lines indicate the position of the Fermi level.

theory, in an electrochemical environment, the distribution of the density of states on the *energy* coordinate can be expressed by:

$$D_H(\varepsilon) = \frac{1}{\pi} \frac{\Delta(\varepsilon)}{[\varepsilon - (\varepsilon_H + \Lambda(\varepsilon) - 2\lambda q)]^2 + \Delta(\varepsilon)^2} \quad (8)$$

$\varepsilon_H$  is the position of the center of  $D_H$ . When the H-atom is far away from the surface, it is the energy level of the orbital 1s.  $\lambda$  is the energy of re-organization of the solvent and  $q$  is the solvent coordinate according to Marcus and Hush [84,85]. We apply the same criterion as in previous works [61], and use a variable value of  $\lambda$  from 3 eV in the bulk of the electrolyte to 1.5 eV at the surface (partial solvation). Obviously, below the surface the value is zero (no solvation, no solvent coupling).

The chemisorption functions  $\Delta(\varepsilon)$  and  $\Lambda(\varepsilon)$  account for the interaction with the metal and produce a broadening and a shift of the electronic states of the H-atom and are given by [82,83]:

$$\begin{aligned} \Delta(\varepsilon) &= \sum_k |V|^2 \pi \delta(\varepsilon - \varepsilon_k) \approx |V|^2 \pi \rho_{Au}(\varepsilon) = \Delta_{sp}(\varepsilon) + \Delta_d(\varepsilon) \\ &= |V_{sp}|^2 \pi \rho_{Au-sp}(\varepsilon) + |V_d|^2 \pi \rho_{Au-d}(\varepsilon) \quad (9a - b) \\ \Lambda(\varepsilon) &= \frac{1}{\pi} P \int \frac{\Delta(\varepsilon')}{\varepsilon - \varepsilon'} d\varepsilon' = \Lambda_{sp}(\varepsilon) + \Lambda_d(\varepsilon). \end{aligned}$$

Here, we consider additive coupling constants:  $|V_{sp}|^2$  and  $|V_d|^2$ , respectively (overlap interaction or hopping integrals between the

electronic states of the 1s state of H-atom  $|1s_H\rangle$  and those of the metal  $|k_{sp/d}\rangle$ :  $V_{sp/d} = \langle k_{sp/d} | \hat{V} | 1s_H \rangle$ ). We have introduced an improvement in our theory and assumed that the coupling constants have an exponential dependence with the energy below the Fermi level instead of being constants:

$$\begin{aligned} |V_{sp/d}|^2 &= V_{sp/d}^0 \exp(a_{sp/d} \varepsilon) & \varepsilon < 0 \\ |V_{sp/d}|^2 &= V_{sp/d}^0 & \varepsilon > 0. \end{aligned} \quad (10)$$

This is an approximate but reasonable energy dependence [86], since the 1s orbital of hydrogen broadens as a result of electron tunneling through the barrier, which is assumed to exist between the adsorbate and the substrate. Thus, one could expect the width  $\Delta(\varepsilon)$ , or tunneling probability, to be proportional to an exponential of the barrier height. Using this approach, we obtained a better fit of the density of states when the hydrogen is near the surface.

In contrast to pure DFT, this theory includes the important solvent fluctuations and allows an explicit inclusion of the electrode potential.

The free energy has been obtained as a function of the distance to the surface and the solvent coordinate  $q$  for the equilibrium potential (overpotential  $\eta = 0$ ). Correlation and exchange terms obtained from DFT have been included as corrections such as described in previous works [61]. As suggested by Ruban et al. [52] an amount of 0.2 eV was added to these values in order to account for the entropy of the hydrogen gas and the zero-point energy of the  $H_2$  molecule.

The solvent coordinate has been normalized in such a way, that a solvent characterized by a coordinate  $q$  would be in equilibrium with a reactant of charge  $-q$ . According to these definitions, we have  $q = 0$  for a neutral H-atom and  $q = -1$  for the charged proton  $H^+$ . The initial state is a strongly-solvated proton ( $q = -1$ ) at large distances from the surface, whose 1s orbital lies above the Fermi level (see Fig. 6a); the final state of the Volmer step is an adsorbed, unsolvated, hydrogen atom with one electron in the 1s state ( $q = 0$ ). DFT yields the PDOS on the 1s orbital of the neutral hydrogen atom at the different positions (along the line for  $q = 0$  in the potential-energy plot of Fig. 6). According to the Marcus–Hush theory [85,86], the reaction occurs when a solvent fluctuation (changes of the solvent coordinate  $q$ ) shifts the valence orbital of the proton to the Fermi level (transition state, see Fig. 6b), where it gets filled, and the resulting hydrogen atom finally is adsorbed (Fig. 6c). The density of states for the hydrogen at different  $q$  can be calculated through Eq. (8) using the chemisorption functions obtained by fitting the PDOS from DFT at  $q = 0$  at the corresponding distance from the surface taking into account the expressions (9a-b) and (10). The energy barrier for this process is about 0.6 eV, being some lower than that for pure Au(111) ( $\approx 0.7$  eV [39,82]). The bimetallic system presents a shift of the *d*-band corresponding to the Au atoms at the surface, as we have already mentioned in the section above, towards higher energies with respect to the pure Au surface. This is already an indicator that the adsorption of hydrogen is stronger than on the pure Au surface, as mentioned above in the previous section. Therefore, one expects an indirect catalytic effect by the presence of the second layer of Pd, which affects the electronic structure of the Au atoms at the surface.

Furthermore, the adsorbed hydrogen can go from this equilibrium position over a barrier of about 0.62 eV (Fig. 6d) and penetrates below the surface up to the Pd layer, where it is absorbed and reaches a new equilibrium position (Fig. 6e). Obviously, inside the metal, the solvent is absent and the energy is independent of the solvent coordinate  $q$ .

At short distances, when the hydrogen starts to penetrate below the surface, it interacts not only with the electronic states of the Au atoms at the surface, but also with those of the second layer of Pd. This is evident from the changes also observed on the *sp*- and *d*-bands of Pd atoms. Besides the electronic states of the 1s orbital of hydrogen, the *sp*- and *d*-states of Pd are represented at the right side of Fig. 6c, d, e. In the region where the 1s states of hydrogen appear, a peak in the *sp*-bands of both Au and Pd is observed due to bond formation. These overlaps increase



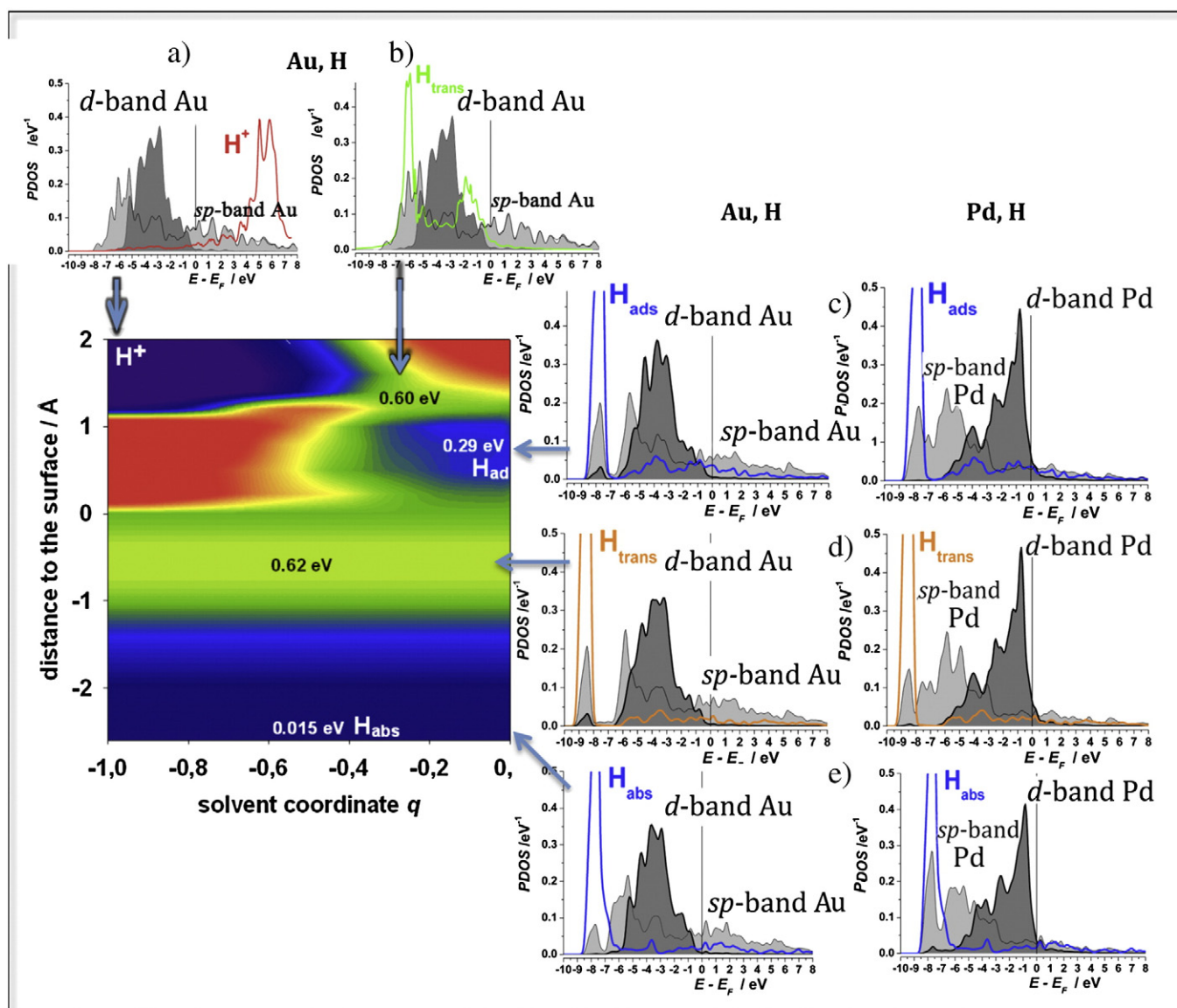


**Fig. 6.** Free energy surface for the Volmer-adsorption reaction and for the further hydrogen absorption on the Pd–Au bimetallic system. The changes on the 1s states of hydrogen and the *sp*- (light gray) and *d*-states (dark gray) of Au and Pd are also shown at different characteristic positions: a) initial state for the Volmer reaction, a solvated  $H^+$  (red) at a large distance from the surface; b) transition state for the Volmer reaction ( $H$ : green); c) final equilibrium state for the Volmer reaction: an adsorbed unsolvated hydrogen atom (blue); d) transition state for the absorption of the hydrogen atom (orange); e) final equilibrium state for the absorption of hydrogen (blue).

for Pd and decrease for Au from c) through d) to e). Electronic charge flows from higher to lower energy regions in order to stabilize the bond between the metal and the hydrogen atom.

At the barrier for the absorption, a gap of around 1 eV appears between the (localized) *sp*-states of Au participating in the bond with hydrogen, and the rest of the *sp*-band (free electrons). This effect is not observed on the electronic states of Pd. Only a small participation in the bond of *d*-states of Pd can be also observed (overlap of a small peak).

Another complementary description of electronic redistribution can be obtained by a more precise analysis of charge differences, as we have already carried out above for the formation of the bimetallic system.

Similarly, we have also calculated electron density changes induced by the absorption of hydrogen according to the following expression:

$$\Delta\rho = \rho_{H-Au/Pd/Au(111)} - \rho_{Au/Pd/Au(111)} - \rho_H. \quad (11)$$

Again,  $\rho_H$  and  $\rho_{H-Au/Pd/Au(111)}$  were calculated using the same coordinates as in the system when the hydrogen is adsorbed.

The results are shown in Fig. 7 for the different positions of the hydrogen, from the adsorption equilibrium to the absorption equilibrium states. Here, the different contribution weights of the first Au layer and second Pd layer to the bond formation during the reaction path become very clear. At the adsorption equilibrium position (0.8 Å) and when the hydrogen is crossing the first Au layer (0.0 Å), the interaction is mainly with Au, although some electronic charge changes on the Pd layer also indicate a participation of this layer.

When the hydrogen goes under the surface and crosses the activation barrier (−0.9 Å) the interaction is almost the same with both layers, Au and Pd. In this case, a strong localization of the charge is observed in agreement with the appearance of the gap in the *sp* band of Au, as mentioned above. Finally, when the hydrogen has reached the equilibrium position for the absorption (−2.6 Å), the interaction is practically restricted to the Pd layer. In the latter case, the third Au layer, specially the Au atom just below the hydrogen, also shows a little contribution. In all the cases, the electronic charge flows into the hydrogen atom.

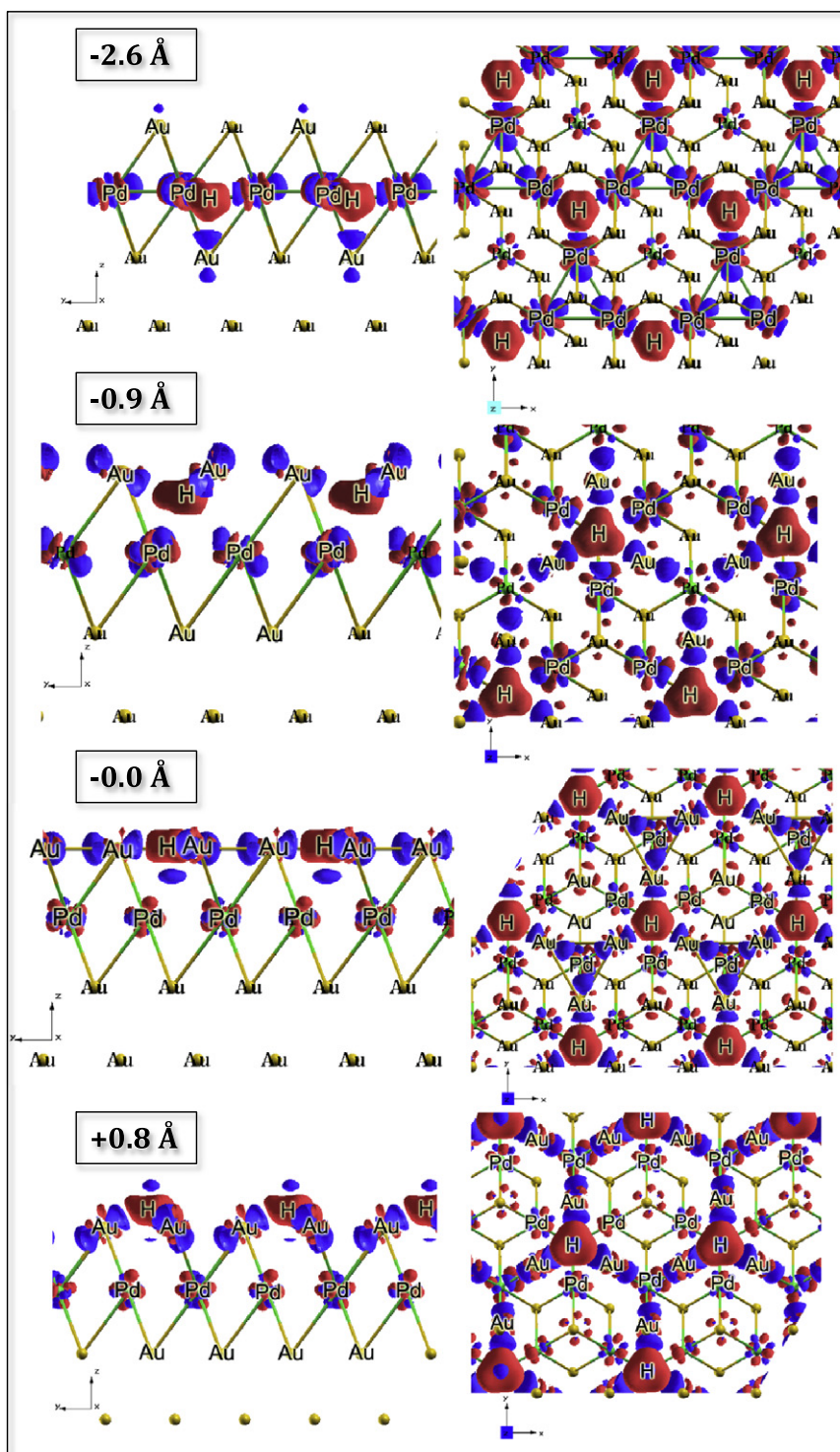


**Fig. 7.** Redistribution of the electronic charge, as obtained from Eq. (11), during the absorption of hydrogen in the Au-Pd bimetallic system. Red and blue colors correspond to electron accumulation and depletion, respectively. The  $0.002 e \text{ \AA}^{-1}$  isosurface has been plotted with the XCrySDen package [77]. The distance of the hydrogen from the surface is indicated for each case.

The values of the Bader charge [87] on the hydrogen are shown at the right axis of Fig. 8 as a function of the  $z$ -coordinate perpendicular to the surface. The plane-averaged charge obtained by integration in the  $xy$ -plane by the formation of the bimetallic system (from Fig. 1, bottom part) is also included for comparison. At larger distances from the surface, the hydrogen is neutral having one electron in its  $1s$  orbital. When it approaches the surface, the electronic charge on it gradually increases up to the equilibrium position.

At the first glance, these results are in contradiction with the decrease on the work function when hydrogen is adsorbed. Indeed, a dipole is expected pointing from the surface to the H atom since the electronegativity of hydrogen is some lower than that of Au (H: 2.20, Au: 2.54). However, similarly as in the case of Ag surfaces [78], it is also evident that the redistribution of electronic charge shows a complicated pattern with accumulation–depletion oscillations (see Fig. 7, upper part). Therefore, it is fictitious to represent the behavior of the

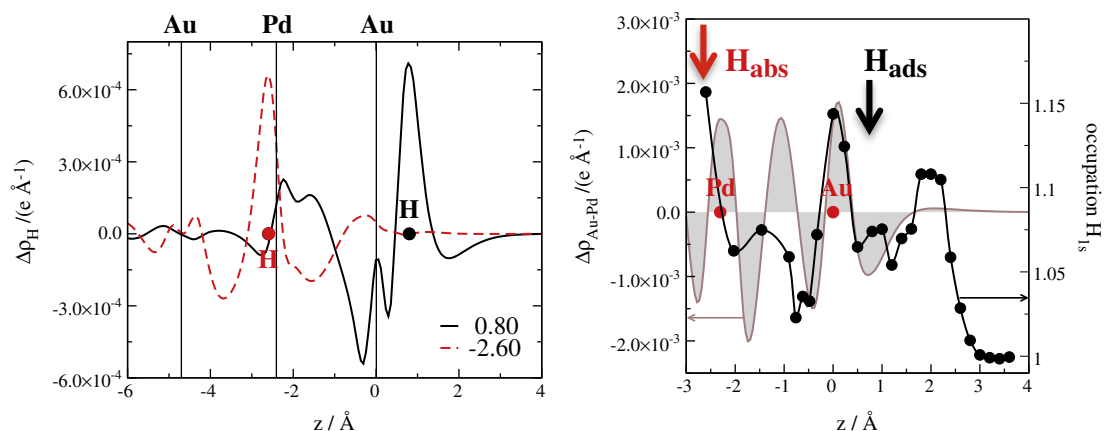


**Fig. 8.** (Left) Averaged planar charge difference calculated with Eq. (11) for hydrogen adsorption (black) and absorption (red) at Au/Pd/Au(111) system. (Right) Occupation of the 1s orbital of hydrogen when it approaches the Au/Pd/Au(111) system. The averaged planar charge difference when the bimetallic Au/Pd/Au(111) system is formed (see Fig. 2, bottom left) is also included for comparison.

systems through ideal dipoles with a well-defined charge separation. There are many examples in the literature that show this anomalous behavior [76,78] that the work function decreases despite the electronegativity of the adatoms. A key point is the slight electronic charge depletion at distances farther out to the surface, which strongly contributes to the observed work function decrease. Although small compared to the electron accumulation layer nearer the surface, it is sufficiently far from the surface to determine the sign of the dipole (see the electronic diminution at about 2 Å in the upper part of Fig. 7).

Similarly like we have mentioned in the discussion of the formation of the bimetallic system above, the distance from the center of the slab weights the dipole. Metallic electronic states extending out into the vacuum become depopulated (see also the small blue cloud over the adsorbed hydrogen in Fig. 7, bottom, left).

The correlation of the changes in the 1s occupation with the oscillation in the redistribution of charge by the alloy formation is also noticeable. The occupation also increases when the hydrogen is absorbed, indicating a tendency to form a hydride-type-bond with the second layer of Pd.

Table 4 summarizes the kinetics and thermodynamics for both adsorption and adsorption processes on the bimetallic system in comparison with the one-component systems. We compare our results for the Au/Pd/Au(111) with data from the literature [88] for Pd(111) and Au(111). The adsorption energy is only slightly lower than on Au(111) and much higher than on Pd(111). On the contrary, the absorption energy is negative like on Pd(111), but slightly higher; it is positive and much higher on Au(111). More interesting, the activation barrier for the absorption is similar (somewhat lower) to that for Pd(111) and much lower than that for Au(111), but for the reverse process (de-absorption) it is much higher than those for Pd(111) and Au(111). This effect makes this system attractive for hydrogen storage applications, since the hydrogen can be kept trapped under the surface Au layer.

**Table 4**

Adsorption/absorption energies and activation energy for hydrogen diffusion from the surface (s) to the subsurface (ss) and from the subsurface to the surface for the **Au/Pd/Au(111)** bimetallic system (bold-faced values) in comparison with previous calculations of the literature for Pd(111) and Au(111) [89]. Experimental values of activation energies for the bulk diffusion of hydrogen (diff) for the two latter systems also are included. Positive values indicate that the process is endothermic. All values are in eV.

System	$\Delta E_{\text{ads}}$	$\Delta E_{\text{abs}}$	$E_{\text{act}}(s \rightarrow \text{ss})$	$E_{\text{act}}(\text{ss} \rightarrow s)$	$\Delta E_{\text{ads-abs}}$	Diff
Pd(111)	-0.6	-0.295	0.4	0.1	0.3	0.23
<b>Au/Pd/Au(111)</b>	<b>0.09</b>	<b>-0.184</b>	<b>0.332</b>	<b>0.606</b>	<b>-0.274</b>	-
Au(111)	0.105	0.735	0.76	0.12	0.54	0.25

Finally, Fig. 9 shows the evolution of the density of states for the hydrogen, when it goes from the adsorption equilibrium position under the surface up to the absorption equilibrium position near the second Pd layer. The maximum of the electronic distribution continuously shifts to higher negative energies when the hydrogen approaches to the barrier. This effect can be mainly attributed to Pauli repulsion, which is expected to be highest at the transition state, where the localization also is maximal (recall the gap in the *sp*-band of Au observed in Fig. 6d and the strong localization of charge redistribution in Fig. 6 (-0.9 Å). After it has crossed the barrier corresponding to the transition state, when the interaction with the Pd layer increases, the peak becomes broader and shifts again to less negative energies due to the increase in the delocalization of electrons.

#### 4. Conclusions

We have considered an ideal bimetallic model-system consisting of a complete monolayer of Pd underneath the top layer of Au(111). We have combined DFT calculations with the electrocatalysis theory to investigate the following properties:

(i) Stability of the system.

The energy calculations show that the system with one Pd submonolayer is more stable than that with one Pd overlayer, and that the binding energy between Pd–Au is much stronger than that between Au–Au. These results are in line with experimental data showing that the topmost layer of Pd–Au alloys consists of pure Au.

(ii) Electronic charge redistribution of the system in *space* and *energy* by alloy formation.

We have observed that the electronic density between the first and second and the second and third layers is larger for the Pd–Au bimetallic system in agreement with the strongest bond as already determined by the energy estimation. Both Au and Pd contribute stronger to this interlayer electronic charge than in the case of the one component system Au(111). It is difficult to distinguish charge transfers because of the internal redistribution of the electronic density when the rehybridization to form the alloy takes place. Although the changes were small, a decrease was observed in the *d* charge and a gain of *sp* charge at the Au site, while a gain in *d* charge of Pd and a loss of *sp* charge were found, in agreement with experiments.

(iii) Thermodynamics for hydrogen adsorption/absorption.

The hydrogen adsorption energy is only slightly lower than on Au(111) and much higher than on Pd(111). On the contrary, the

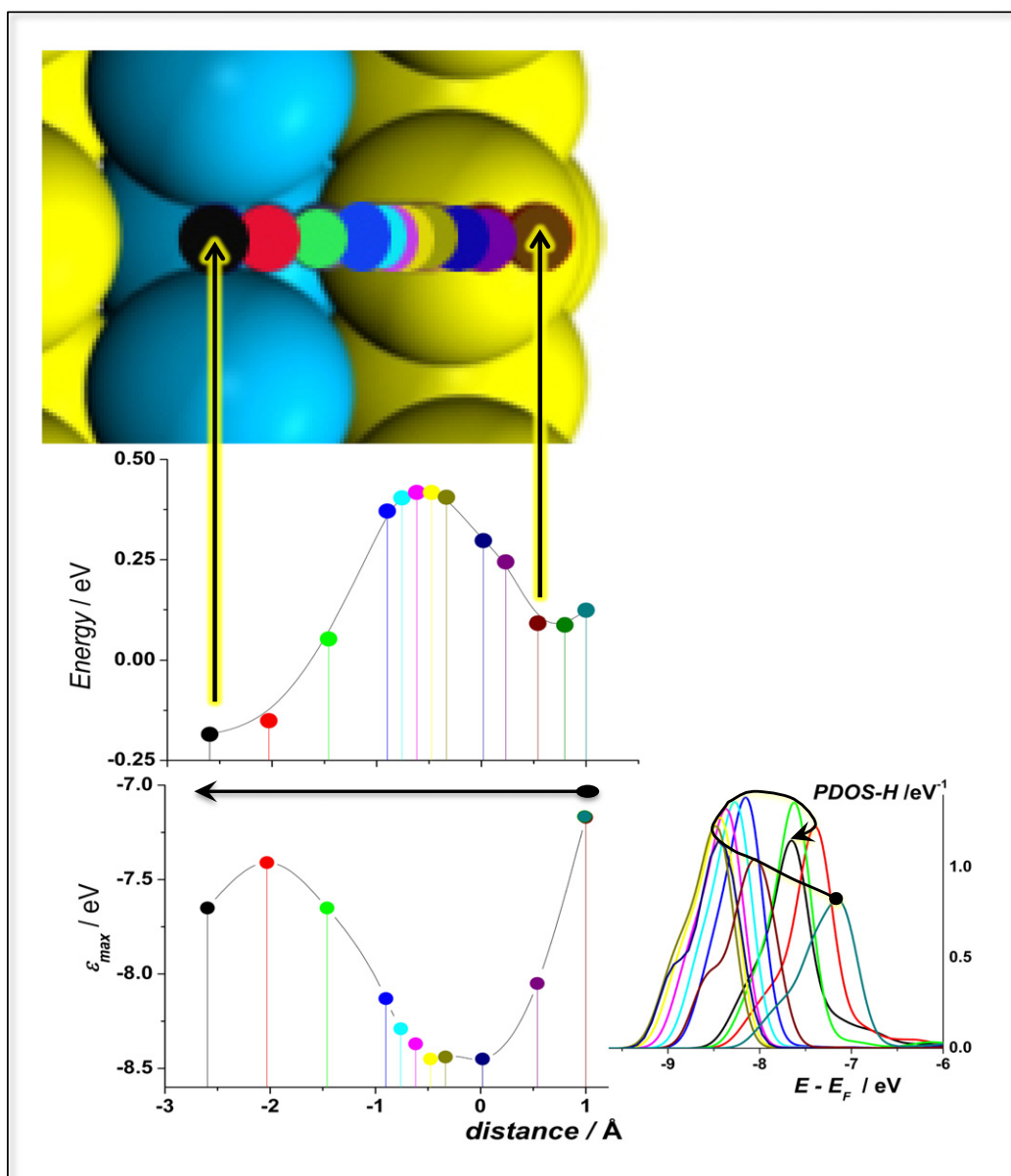


Fig. 9. Energy obtained by DFT ( $q = 0$ ) for the hydrogen absorption process at different distances from the surface (upper plot). Maximum position (bottom part, left) at different distances from the surface of the distribution of  $1s$  electronic states of hydrogen (bottom part, right).

absorption energy is negative like on Pd(111), but this process is somewhat less favorable.

(iv) Kinetics for hydrogen adsorption/absorption.

The activation barrier for the Volmer reaction has been found only slightly lower than for Au(111).

More interesting, the activation barrier for the absorption is slightly lower than that for Pd(111) and much lower than that for Au(111), but for the de-absorption it is much higher than those for Pd(111) and Au(111). This effect makes this system attractive for hydrogen storage applications.

#### Acknowledgements

This work is part of the research network financed by the Deutsche Forschungsgemeinschaft FOR1376 and the DAAD-PHC PROCOPE 2011 Project No. 25099UB. The content has been presented and discussed

in the internal meeting of these networks. E.S. acknowledges PIP-CONICET 112-201001-00411 and PICT-2012-2324 (Agencia Nacional de Promoción Científica y Tecnológica, FONCYT, préstamo BID). A generous grant of computing time from the Baden-Württemberg grid is gratefully acknowledged.

This work was performed using HPC resources from GENCI-[CCRT/CINES/IDRIS] (Grant 2012-[x2012082022]) and the CCRE of Université Pierre et Marie Curie.

Finally, fruitful discussions with Prof. W. Schmickler and Prof. R. Nazmutdinov are gratefully acknowledged.

#### Appendix A. Supplementary data

Supplementary data to this article can be found online at <http://dx.doi.org/10.1016/j.susc.2014.06.015>.

## References

- [1] H. Baltruschat, S. Ernst, N. Bogolowski, *Electrocatalysis at Bimetallic Surfaces Obtained by Surface Decortion*, in: E. Santos, W. Schmickler (Eds.), *Catalysis in Electrochemistry, From Fundamentals to Strategies for Fuel Cell Development*, Wiley, Hoboken, 2011, (Ch. 9).
- [2] V. Ponec, *Appl. Catal. A* 222 (2001) 31.
- [3] R.J. Behm, *Z. Phys. Chem.* 223 (2009) 9.
- [4] M.S. Chen, K. Luo, T. Wei, Z. Yan, D. Kumar, C.-W. Yi, D.W. Goodman, *Catal. Today* 117 (2006) 37.
- [5] J.K. Edwards, G.J. Hutchings, *Angew. Chem. Int. Ed.* 47 (2008) 9192.
- [6] T.B. Massalski, *Binary Alloy Phase Diagram*, 2nd ed. ASM International, Materials Park, OH, 1990.
- [7] M.H.F. Sluiter, C. Colinet, A. Pasturel, *Phys. Rev. B* 73 (2006) 174204.
- [8] S.V. Barabash, V. Blum, S. Müller, A. Zunger, *Phys. Rev. B* 74 (2006) 035108.
- [9] F.R. de Boer, R. Boom, W.C.M. Mattens, A.R. Miedema, A.K. Niessen, *Cohesion in Metals*, North-Holland, Amsterdam, 1988.
- [10] J. Kuntze, S. Speller, W. Heiland, A. Atrei, U. Bardi, *Phys. Rev. B* 60 (1999) 9010.
- [11] C.-W. Yi, K. Luo, T. Wei, D.W. Goodman, *J. Phys. Chem. B* 109 (2005) 18535.
- [12] H.J. Gotsis, I. Rivalta, E. Sicilia, N. Russo, *Chem. Phys. Lett.* 468 (2009) 162.
- [13] E. Budevski, G. Staikov, W.J. Lorenz, *Electrochemical Phase Formation and Growth – An Introduction to the Initial Stages of Metal Deposition*, VCH, Weinheim, 1996.
- [14] Z. Li, F. Gao, Y. Wang, F. Calaza, L. Burkholder, W.T. Tysoe, *Surf. Sci.* 601 (2007) 1898.
- [15] R. Ferrando, J. Jellinek, R.L. Johnston, *Chem. Rev.* 108 (2008) 846.
- [16] X. Liu, D. Tian, Ch. Meng, *Comput. Theoret. Chem.* 999 (2012) 246.
- [17] R. Callejas-Tovar, W. Liao, H. Mera, P.B. Balbuena, *J. Phys. Chem. C* 115 (2011) 23758.
- [18] R. Marchal, A. Genest, S. Krüger, N. Rösch, *J. Phys. Chem. C* 117 (2013) 21810.
- [19] B. Zhu, Y. Wang, I.S. Atanasov, D. Cheng, M. Hou, *J. Phys. D: Appl. Phys.* 45 (2012) 165302.
- [20] F. Gao, D.W. Goodman, *Chem. Soc. Rev.* 41 (2012) 8009.
- [21] J. Greeley, M. Mavrikakis, *Nat. Mater.* 3 (2004) 810.
- [22] A. Michaelides, *Surf. Sci.* 601 (2007) 3529.
- [23] J.R. Kitchin, J.K. Nørskov, M.A. Barteau, J.G. Chen, *Phys. Rev. Lett.* 93 (2004) 156801.
- [24] F. Calleja, V.M. García-Suárez, J.J. Hinarejos, J. Ferrer, A.L. Vázquez de Parga, R. Miranda, *Phys. Rev. B* 71 (2005) 125412.
- [25] E. Santos, P. Quaino, W. Schmickler, *Electrochim. Acta* 55 (2010) 4346.
- [26] N.F. Mott, H. Jones, *The Theory of the Properties of Metals and Alloys*, Dover Publ., Inc., NY, 1958.
- [27] E.A. Stern, *Phys. Rev.* 157 (1967) 544.
- [28] S. Raimes, *J. Phys. Radium* 23 (1969) 639.
- [29] H. Piao, N.S. McIntyre, G. Beamson, M.-L. Abel, J.F. Watts, *J. Electron. Spectrosc. Relat. Phenom.* 125 (2002) 35.
- [30] T.-Uh. Nahm, R. Jung, J.-Y. Kim, W.-G. Park, S.-J. Oh, *Phys. Rev. B* 58 (1998) 9817.
- [31] Y.-S. Lee, Y. Jeon, Y.-D. Chung, K.-Y. Lim, Ch.-N. Whang, S.-J. Oh, *J. Korean Phys. Soc.* 37 (2000) 451.
- [32] G. Meitzner, J.H. Sinfelt, *Catal. Lett.* 30 (1995) 1.
- [33] A. Roudgar, A. Groß, *J. Electroanal. Chem.* 548 (2003) 121.
- [34] A. Roudgar, A. Groß, *Phys. Rev. B* 67 (2003) 033409.
- [35] E. Santos, P. Quaino, P.F. Hindelang, W. Schmickler, *J. Electroanal. Chem.* 649 (2010) 149.
- [36] L.A. Kibler, *Electrochim. Acta* 53 (2008) 6824.
- [37] L.A. Kibler, A.M. El-Aziz, R. Hoyer, D.M. Kolb, *Angew. Chem. Int. Ed.* 44 (2005) 2080.
- [38] L.M.C. Pinto, G. Soldano, A.F. Innocente, A.C.D. Angelo, E. Santos, W. Schmickler, *Catal. Today* 202 (2013) 191.
- [39] G. Soldano, E.N. Schulz, D.R. Salinas, E. Santos, W. Schmickler, *Phys. Chem. Chem. Phys.* 13 (2011) 16437.
- [40] P. Quaino, E. Santos, H. Wolfschmidt, M.A. Montero, U. Stimming, *Catal. Today* 177 (2011) 55.
- [41] W. Schmickler, E. Santos, P. Quaino, G. Soldano, P. Hindelang, E. Schulz, *ChemPhysChem* 12 (2011) 2274.
- [42] H. Guesmi, C. Louis, L. Delannoy, *Chem. Phys. Lett.* 503 (2011) 97.
- [43] A. Dhoubi, H. Guesmi, *Chem. Phys. Lett.* 521 (2012) 98.
- [44] G. Laurent, H.F. Busnengo, P. Rivière, F. Martin, *Phys. Rev. B* 77 (2008) 193408.
- [45] L.A. Mancera, R.J. Behm, A. Groß, *Phys. Chem. Chem. Phys.* 15 (2013) 1497.
- [46] Y. Ma, T. Diemant, J. Bansmann, R.J. Behm, *Phys. Chem. Chem. Phys.* 13 (2011) 10741.
- [47] S. Ogura, M. Okada, K. Fukutani, *J. Phys. Chem. C* 117 (2013) 9366.
- [48] L. Piccolo, A. Piednoir, J.-C. Bertolini, *Surf. Sci.* 600 (2006) 4211.
- [49] W.-Y. Yu, G. Mullen, C.B. Mullins, *J. Phys. Chem. C* 117 (2013) 19535.
- [50] M. Takahashi, Y. Hayashi, J. Mizuki, K. Tamura, T. Kondo, H. Naohara, K. Uosaki, *Surf. Sci.* 461 (2000) 213.
- [51] L.A. Kibler, M. Kleinert, V. Lazarescu, D.M. Kolb, *Surf. Sci.* 498 (2002) 175.
- [52] A. Ruban, B. Hammer, P. Stoltze, H.L. Skriver, J.K. Nørskov, *J. Mol. Catal. A* 115 (1997) 421.
- [53] M.I. Rojas, M.G. Del Pópolo, E.P.M. Leiva, *Langmuir* 16 (2000) 9539.
- [54] M. Baldauf, D.M. Kolb, *Electrochim. Acta* 38 (1993) 2145.
- [55] I.A. Pašti, N.M. Gavrilov, S.V. Mentus, *Hydrogen Adsorption on Palladium and Platinum Overlayers: DFT Study*, *Adv. in Phys. Chem. Hindawi Publ. Corp.*, 2011, (ID 305634).
- [56] M.E. Björketun, G.S. Karlbert, J. Rossmeisl, I. Corkendorff, H. Wolfschmidt, U. Stimming, J.K. Nørskov, *Phys. Rev. B* 84 (2011) 045407.
- [57] Y. Pluntke, L.A. Kibler, D.M. Kolb, *Phys. Chem. Chem. Phys.* 10 (2008) 3684.
- [58] S. Pandelov, E. Stimming, *Electrochim. Acta* 52 (2007) 5548.
- [59] B. Zhu, G. Thrimurthu, L. Delannoy, C. Louis, C. Mottet, J. Creuze, B. Legrand, H. Guesmi, *J. Catal.* 308 (2013) 272.
- [60] E. Santos, W. Schmickler, *Angew. Chem. Int. Ed.* 46 (2007) 8262.
- [61] E. Santos, A. Lundin, K. Pötting, P. Quaino, W. Schmickler, *Phys. Rev. B* 79 (2009) (235436-1-235436-10).
- [62] B. Hammer, L.B. Hansen, J.K. Nørskov, *Phys. Rev. B* 59 (1999) 7413.
- [63] G. Kresse, J. Hafner, *Phys. Rev. B* 47 (1993) 558.
- [64] G. Kresse, J. Hafner, *Phys. Rev. B* 49 (1994) 14251.
- [65] J.P. Perdew, J.A. Chevary, S.H. Vosko, K.A. Jackson, M.R. Pederson, D.J. Singh, C. Fiolhais, *Phys. Rev. B* 46 (1992) 6671.
- [66] C. Kittel, *Introduction to Solid State Physics*, Third ed. Wiley, New York, 1967.
- [67] T.V. de Bocarmé, T.-D. Chau, F. Tielens, J. Andrés, P. Gaspard, L.R.C. Wang, H.J. Kreuzer, N. Kruse, *J. Chem. Phys.* 125 (2006) 054703.
- [68] F. Tielens, J. Andrés, *J. Phys. Chem. C* 111 (2007) 10342.
- [69] F. Tielens, M. Trejda, M. Ziolk, S. Dzwigaj, *Catal. Today* 139 (2008) 221.
- [70] J.P. Perdew, K. Burke, M. Ernzerhof, *Phys. Rev. Lett.* 77 (1996) 3865.
- [71] J.P. Perdew, K. Burke, M. Ernzerhof, *erratum Phys. Rev. Lett.* 78 (1997) 1396.
- [72] P.E. Blöchl, O. Jepsen, O.K. Andersen, *Phys. Rev. B* 49 (1994) 16223.
- [73] G. Kresse, J. Joubert, *Phys. Rev. B* 59 (1999) 1758.
- [74] H.J. Monkhorstand, J.D. Pack, *Phys. Rev. B* 13 (1976) 5188.
- [75] L. Bengtsson, *Phys. Rev. B* 59 (1999) 12301.
- [76] T.C. Leung, C.L. Kao, W.S. Su, Y.J. Feng, C.T. Chan, *Phys. Rev. B* 68 (2003) 195408.
- [77] A. Kokalj, *Comput. Mater. Sci.* 28 (2003) 155; *XCrySDen*, *J. Mol. Graph. Model.* 17 (1999) 176 (Code available from <http://www.xcrysden.org/>).
- [78] M.J. Juárez, E. Santos, *J. Phys. Chem. C* 117 (2013) 4606.
- [79] N.D. Orf, I.D. Baikie, O. Shapira, Y. Fink, *Appl. Phys. Lett.* 94 (2009) 113504.
- [80] R. Fischer, Th. Fauster, *Surf. Rev. Lett.* 3 (1996) 1783.
- [81] E. Santos, P. Quaino, W. Schmickler, *Phys. Chem. Chem. Phys.* 14 (2012) 11224.
- [82] P.W. Anderson, *Phys. Rev.* 124 (1961) 41.
- [83] D.M. Newns, *Phys. Rev.* 178 (1969) 1123.
- [84] R.A. Marcus, *J. Chem. Phys.* 24 (1956) 966.
- [85] N.S. Hush, *J. Chem. Phys.* 28 (1958) 962.
- [86] J.W. Gadzuk, J.K. Hartman, T.N. Rhodin, *Phys. Rev. B* 4 (1971) 241.
- [87] R.F.W. Bader, P.E. Cade, P.M. Beddall, *J. Amer. Chem. Soc.* 93 (1971) 3095.
- [88] P. Ferrin, S. Kandoi, A.U. Nilekar, M. Mavrikakis, *Surf. Sci.* 606 (2012) 679.